ADVANCED ENERGY MATERIALS
www.advenergymat.de

Liquid-Like Ionic Conduction in Solid Lithium and Sodium Monocarba-*closo*-Decaborates Near or at Room Temperature

Wan Si Tang, Motoaki Matsuo, Hui Wu, Vitalie Stavila, Wei Zhou, Albert Alec Talin, Alexei V. Soloninin, Roman V. Skoryunov, Olga A. Babanova, Alexander V. Skripov, Atsushi Unemoto, Shin-Ichi Orimo,* and Terrence J. Udovic**

An avid search is underway for solid electrolytes with sufficiently high ionic conductivities and stabilities to enable the commercial viability of all-solid-state rechargeable batteries. Recently, we discovered a novel class of superionic solid electrolytes, whose facile cation conduction pathways are enabled by the spacious, vacancy-rich, interstitial network afforded by a sublattice of overly large, polyhedral, orientationally mobile, *closo*-borate anions (e.g., $B_{12}H_{12}^{2-}$ and $B_{10}H_{10}^{2-}$).[1–4] Indeed, above their entropically driven, order–disorder phase-transition temperatures (T_{trans}), the sodium salts of polycrystalline $Na_2B_{12}H_{12}$ and $Na_2B_{10}H_{10}$ were shown to exhibit respective conductivities of around 0.1 S cm^{-1} (above $T_{trans} \approx 529$ K)[3] and 0.01 S cm^{-1} (above $T_{trans} \approx 380$ K).[4] Both $Li_2B_{12}H_{12}$ and $Li_2B_{10}H_{10}$ have much higher transition temperatures in excess of 600 K, likely accompanied by superionic conduction, but also prone to significant decomposition.[1,2,5,6] In an effort to find related chemically modified materials with lower, more-device-relevant, transition temperatures, we very recently extended our work to include the $MCB_{11}H_{12}$ (M = Li, Na) lithium and sodium salts, which contain the $B_{12}H_{12}^{2-}$-analogous, monovalent, icosahedral $CB_{11}H_{12}^{-}$ anion.[7] Both compounds exhibited superionic conductivities surpassing 0.1 S cm^{-1} above their order–disorder phase transitions near 400 K and 380 K, respectively, which are significant improvements compared to their divalent-anion-based $Na_2B_{12}H_{12}$ and $Li_2B_{12}H_{12}$ cousins. This suggests that the monovalency of the anion and the resulting 1:1 cation:anion stoichiometric ratio may be highly preferable for enhancing cation mobility and minimizing T_{trans} compared to anion divalency and a 2:1 cation:anion ratio.

These results led us to explore the related MCB_9H_{10} (M = Li, Na) lithium and sodium salts, which contain the $B_{10}H_{10}^{2-}$-analogous, monovalent, bicapped-square-antiprismatic $CB_9H_{10}^{-}$ anion (see **Figure 1**).[8] To form this 1-carba-*closo*-decaborate anion, one of the apical {B-H} vertices of the $B_{10}H_{10}^{2-}$ anion is replaced by an isoelectronic {C—H} group, thus again leading to a unity reduction in valency, as for $CB_{11}H_{12}^{-}$. Here we show that the chemically similar $LiCB_9H_{10}$ and $NaCB_9H_{10}$ salts both exhibit noticeably lower respective T_{trans} values near or below room temperature, not only compared to $Li_2B_{10}H_{10}$ and $Na_2B_{10}H_{10}$, but also compared to $LiCB_{11}H_{12}$ and $NaCB_{11}H_{12}$. These lower structural transitions lead to liquid-like ionic conductivities for $LiCB_9H_{10}$ (0.03 S cm^{-1} at 354 K) and $NaCB_9H_{10}$ (0.03 S cm^{-1} at 297 K).

Figure 2 indicates hysteretic phase changes for both $LiCB_9H_{10}$ and $NaCB_9H_{10}$ based on the respective endothermic (upon heating) and exothermic (upon cooling) differential scanning calorimetry (DSC) features. For each compound, two features are evident, suggesting that there is a two-stage phase transformation occurring, presumably from an ordered phase at lower temperatures to two progressively more disordered phases at higher temperatures. For $LiCB_9H_{10}$, the onsets of these disordered phases occur roughly at 332 K and 342 K upon heating and their transformations back start roughly at 344 K and 334 K upon cooling. For $NaCB_9H_{10}$, the onsets occur roughly at 290 K and 310 K upon heating, and unlike for $LiCB_9H_{10}$, the back-transformation upon cooling appears to largely bypass the intermediate transition, occurring in a single step (below room temperature) starting roughly at 285 K. These transitions are clearly lower than their respective $Li_2B_{10}H_{10}$, $LiCB_{11}H_{12}$, $Na_2B_{10}H_{10}$, and $NaCB_{11}H_{12}$ analogs,[1,7] rendering

Dr. W. S. Tang
Department of Materials Science and Engineering
University of Maryland
College Park, MD 20742-2115, USA
E-mail: wansi.tang@nist.gov

Dr. W. S. Tang, Dr. H. Wu, Dr. W. Zhou, Dr. T. J. Udovic
NIST Center for Neutron Research
National Institute of Standards and Technology
Gaithersburg, MD 20899-6102, USA
E-mail: udovic@nist.gov

Dr. M. Matsuo, Prof. S. Orimo
Institute for Materials Research
Tohoku University
Sendai 980-8577, Japan
E-mail: orimo@imr.tohoku.ac.jp

Dr. V. Stavila, Dr. A. A. Talin
Energy Nanomaterials
Sandia National Laboratories
Livermore, CA 94551, USA

Dr. A. V. Soloninin, R. V. Skoryunov, Dr. O. A. Babanova, Dr. A. V. Skripov
Institute of Metal Physics
Ural Branch of the Russian Academy of Sciences
Ekaterinburg 620990, Russia

Dr. A. Unemoto, Prof. S. Orimo
WPI-Advanced Institute for Materials Research
Tohoku University
Sendai 980-8577, Japan

DOI: 10.1002/aenm.201502237

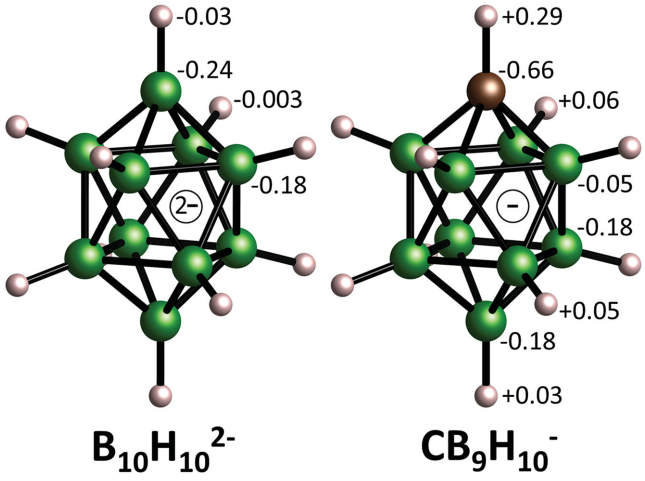

Figure 1. Related geometries of the $B_{10}H_{10}^{2-}$ and $CB_9H_{10}^-$ anions, with green, brown, and white spheres denoting boron, carbon, and hydrogen atoms, respectively. Mulliken charges, determined by first-principles calculations, are indicated for the structurally distinct atoms of the isolated anions.

them potentially more favorable as practical solid electrolyte materials. Additional DSC thermogravimetric analysis measurements indicate that they both decompose above ≈623–673 K.

X-ray powder diffraction (XRPD) patterns for $LiCB_9H_{10}$ and $NaCB_9H_{10}$ for a sequence of temperatures are shown in Figure S1 (Supporting Information). For both $LiCB_9H_{10}$ and $NaCB_9H_{10}$, the XRPD patterns for the ordered structures are distinct from those for the higher-temperature disordered structures. Although we have yet to solve the structural details of these ordered phases, the distribution of Mulliken charges for the $CB_9H_{10}^-$ anion shown in Figure 1 suggests that the anomalously higher positive charge on the apical H atom covalently bonded to the C atom compared to the other H atoms will likely influence the anion orientations with respect to the surrounding cations, similar to what was observed for $LiCB_{11}H_{12}$ and $NaCB_{11}H_{12}$.[7]

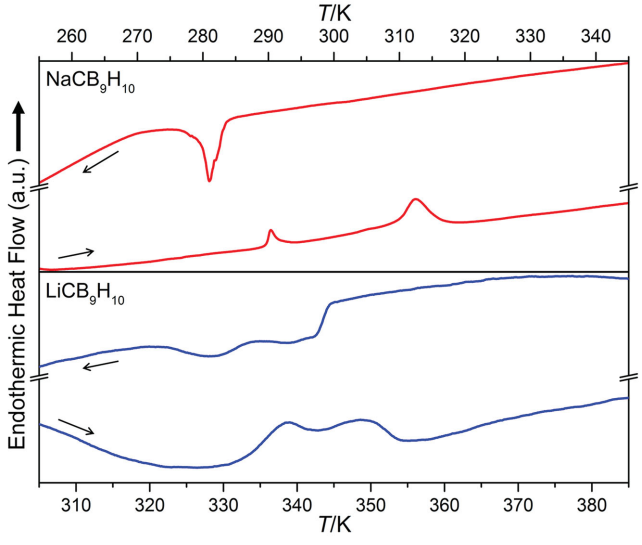

Figure 2. Sequential heating/cooling (±5 K min^{-1}) DSC scans for $LiCB_9H_{10}$ and $NaCB_9H_{10}$. Arrows denote heating and cooling segments.

In those cases, the $CB_{11}H_{12}^-$ anions were oriented so that the considerably more positive C-bonded H atom could avoid close proximity to the neighboring cations.

Figure 3 shows the proposed structure models for two different disordered phases of $LiCB_9H_{10}$ indexed from the 333 K and 383 K XRPD patterns (Figure S2 and S3, Supporting Information), which correspond to the two stages of transformation indicated by the DSC results. The intermediate 333 K structure is believed to be a partially disordered (with respect to anion orientations) orthorhombic structure, which transforms to the more fully disordered hexagonal structure, as evidenced at 383 K. In the orthorhombic structure, the $CB_9H_{10}^-$ anions are orientationally disordered around their local C_4 symmetry axes, but these axes indeed still maintain a specific orientation within the *bc* plane of the structure, slightly canted away from the *b* direction, presumably to minimize interactions between the C-bonded H atoms and the neighboring cations. The centers of the largest interstices for possible Li^+ siting in the structure are indeed farthest from the C-bonded H atoms. Based on the quality of the present XRPD data, we cannot yet totally rule out the possibility that the anions in this intermediate structure are still orientationally ordered. Yet, one might expect any transformation from a fully ordered low-temperature structure to be driven by a significant entropy increase, which is more in line with a structure possessing some discrete change toward anion orientational disorder.

Upon further transformation to disordered hexagonal symmetry at higher temperature, the anions lose all orientational specificity, accommodated as essentially spherically shaped entities now requiring a somewhat expanded unit cell. In both structures, the disordered locations of the light cations could not be definitively ascertained from the XRPD data, although likely locations based on the size of the interstices are depicted in Figure 3. More rigorous structure determinations with specific cation site locations will require synchrotron XRPD as well as complementary neutron powder diffraction data using special ^{11}B, D, and ^7Li-enriched compounds. The hexagonal symmetry for the fully disordered phase is different than the face-centered-cubic (fcc) and body-centered-cubic (bcc) symmetries found for other disordered polyhedral borate systems[1,4,5,7,9] (although we have also observed hexagonal polymorphs for disordered $NaCB_{11}H_{12}$).[7] Disordered $NaCB_9H_{10}$ (Figure S4, Supporting Information) was found to be isostructural with disordered hexagonal $LiCB_9H_{10}$ with a slightly larger unit cell (353 K; a = 6.844 Å, c = 10.908 Å, V = 442.5 $Å^3$). Although we searched for an analogous intermediate orthorhombic structure as for $LiCB_9H_{10}$, we could not find any clear evidence of such a phase from the present XRPD data, even though the DSC scans in Figure 2 suggested that an intermediate phase may exist. XRPD confirmed that $NaCB_9H_{10}$ was in its disordered phase at room temperature upon cooling from higher temperatures as well as upon warming from lower temperatures, although in the latter case, the order–disorder transformation was typically not complete.

The cation jump motions in $LiCB_9H_{10}$ and $NaCB_9H_{10}$ were investigated by ^7Li and ^{23}Na NMR measurements. **Figure 4** shows the behaviors of the ^7Li and ^{23}Na spin-lattice relaxation rates R_1^{Li} and R_1^{Na} measured at the respective resonance frequencies of 28 MHz and 23 MHz near the phase transitions. First considering $NaCB_9H_{10}$, the ^{23}Na relaxation rate exhibits a

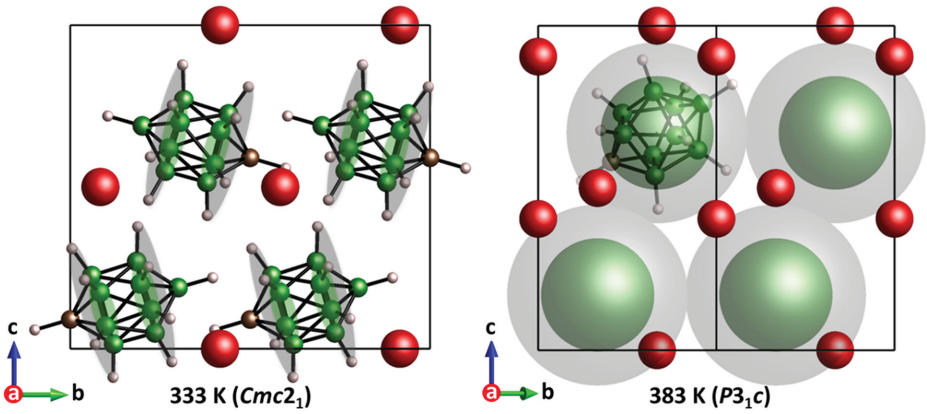

Figure 3. Proposed structures viewed down the *a* axes for disordered $LiCB_9H_{10}$ at 333 K (orthorhombic; $Cmc2_1$; $a = 6.807$ Å, $b = 11.819$ Å, $c = 10.604$ Å, $V = 853.0$ Å^3) and 383 K (hexagonal; $P3_1c$; $a = 6.829$ Å, $c = 10.754$ Å, $V = 434.3$ Å^3) derived from XRPD data. Red, brown, green, and white atoms denote Li, C, B, and H, respectively. For the orthorhombic structure, shaded green and gray regions mimic anion orientational disorder around the anion C_4 symmetry axes. For the hexagonal structure, large green and gray spheres denote the diffraction-average spherical shells of scattering from B/C and H atoms, respectively, associated with the more isotropically (orientationally) disordered anions. N.B., one arbitrarily oriented $CB_9H_{10}^-$ anion in the hexagonal structure is superimposed to aid the reader.

jump between 306 and 315 K upon heating, accompanied by a change in the sign of its temperature dependence. This behavior indicates that the transition from the low-T ordered to high-T disordered phase leads to an abrupt increase in the cation jump rate τ_d^{-1}. Similar behavior of R_1^{Na} corresponding to "folding" of the relaxation rate peak was previously observed near the order–disorder phase transitions in $Na_2B_{12}H_{12}$[2] and $Na_2B_{10}H_{10}$.[4] On the high-T slope of the peak, R_1^{Na} should be proportional to τ_d. Therefore, this slope is determined by the activation energy for cation jumps in the high-T phase. An Arrhenius fit to the high-T data yields an activation energy of 153(7) meV. Upon cooling, the $R_1^{Na}(T)$ data indicate the continuation of the disordered-phase behavior down to at least 283 K, in agreement with the DSC and XRPD data.

For $LiCB_9H_{10}$, the ^{7}Li spin-lattice relaxation rate R_1^{Li} also changes the sign of its temperature dependence in the range 332–350 K. However, the changes in R_1^{Li} near the phase transition in $LiCB_9H_{10}$ are not as sharp as those for R_1^{Na} in $NaCB_9H_{10}$ and are much less hysteretic in the phase-transition region, again consistent with the DSC data. The activation energy derived from the Arrhenius fit to the $R_1^{Li}(T)$ data in the high-T hexagonal phase is 55(9) meV, only about one-third as large as for $NaCB_9H_{10}$. As also observed for $LiCB_{11}H_{12}$ and $NaCB_{11}H_{12}$,[10] this relatively lower activation energy for $LiCB_9H_{10}$ may be attributed to a roughly 25% smaller ionic radius for Li^+ compared to that for Na^+.[11] Since both materials have similarly dimensioned interstitial lattices formed by the $CB_9H_{10}^-$ anions, it is reasonable to assume that the motional barriers for the smaller Li^+ cations through the comparable interstitial channels will be lower than those for the substantially larger Na^+ cations.

For both samples, due to the "folded" natures of the $R_1^{Na}(T)$ and $R_1^{Li}(T)$ peaks, we cannot reliably determine the absolute values of τ_d^{-1}. We can only conclude that the respective Na^+ and Li^+ jump rates exceed $\approx 1.5 \times 10^8$ s^{-1} and $\approx 2 \times 10^8$ s^{-1} above the phase transitions. Moreover, the very narrow ^{23}Na and ^{7}Li NMR lines observed in the high-T phases (<1 kHz fwhm) indicate that fast long-range cation diffusion is indeed occurring.

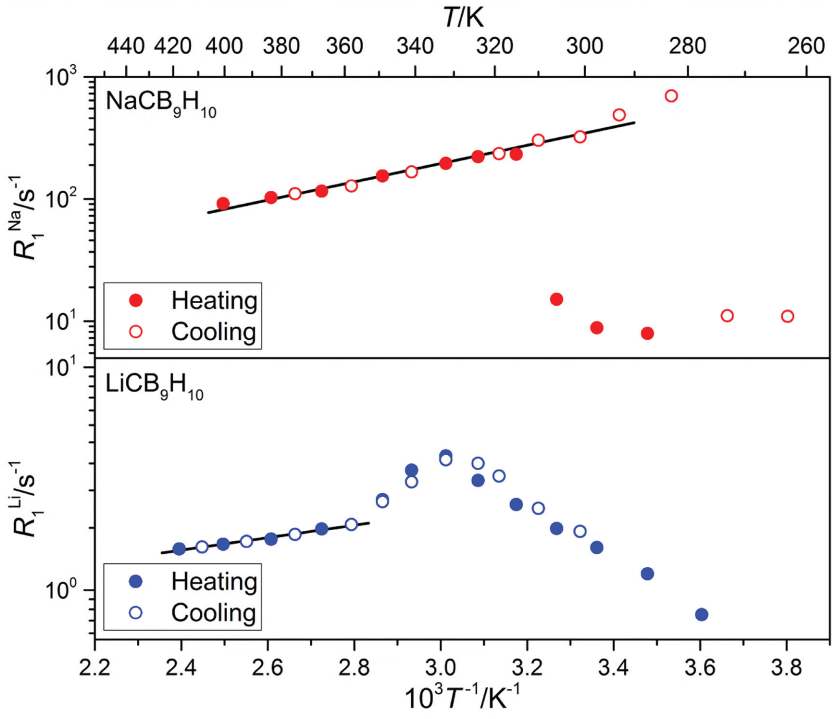

Figure 4. ^{23}Na and ^{7}Li spin-lattice relaxation rates versus the inverse temperature for $NaCB_9H_{10}$ and $LiCB_9H_{10}$ measured at 23 MHz and 28 MHz, respectively, upon heating and cooling. The solid lines show the Arrhenius fits to the data in the ranges 293–401 K ($NaCB_9H_{10}$) and 358–418 K ($LiCB_9H_{10}$).

Anion orientational mobilities in the disordered hexagonal phases of $LiCB_9H_{10}$ and $NaCB_9H_{10}$ were assessed by following the associated H dynamics with quasielastic neutron scattering (QENS) measurements. In contrast to relatively "immobile" anions in their ordered phases, high anion orientational mobilities were clearly evident above their order–disorder phase transitions. The associated quasielastic scattering at all neutron momentum transfers Q was better fit to two Lorentzian components with order-of-magnitude differences in widths (see Figure S5, Supporting Information). For example, $NaCB_9H_{10}$ at 410 K at the lower Q values could be fit to two Lorentzians with linewidths w of around 80 μeV and 1 meV fwhm, which correspond to distinctly different reorientational jump rates ($\tau_1^{-1} = w/(2\,)$) of $\approx 6 \times 10^{10}$ and $\approx 8 \times 10^{11}$ s^{-1}, likely orders of magnitude higher than the cation diffusive jump rates discussed above. Both Lorentzian linewidths tended to increase with Q, which is expected for a reorientational mechanism involving small angular jumps.[12] We speculate that the respective large and small jump rates reflect a combination of small-angle reorientations around the anion C_4 symmetry axes and 180° flips of the anions perpendicular to these axes, but more extensive QENS measurements will be required to confirm this. The narrower Lorentzian linewidth decreased to ≈60 μeV at 370 K, which is roughly 50% higher than that observed for $Na_2B_{10}H_{10}$ at 375 K,[4] thus implying relatively higher anion mobility for $NaCB_9H_{10}$. The 410 K Lorentzian linewidths for $LiCB_9H_{10}$ were found to be roughly 20%–25% smaller than those for $NaCB_9H_{10}$, suggesting slightly less orientationally mobile anions.

Figure 5 summarizes the conductivity-related results for both compounds, which are in line with the fast cation diffusion behavior for the disordered phases observed by NMR. Figure S6 (Supporting Information) shows the typical AC impedance spectra of the Au-symmetric cell for $LiCB_9H_{10}$. They consist of an arc in the high-frequency region and a spike in the low-frequency region due to contributions from the bulk and grain boundaries and the electrode, respectively, indicating characteristics of a pure ionic conductor. Upon temperature increase, the conductivities jump for both materials accompanied by the order–disorder transitions completed by 353 K for $LiCB_9H_{10}$ and 323 K for $NaCB_9H_{10}$, and resulting in superionic conductivities approaching 0.1 S cm^{-1} at 383 K for $LiCB_9H_{10}$ and exceeding 0.1 S cm^{-1} at 373 K for $NaCB_9H_{10}$. It should be noted that a conductivity of 0.03 S cm^{-1} is attained even after cooling to 297 K for $NaCB_9H_{10}$ due to the stable high-T disordered structure, as evidenced by the DSC and NMR results, while there is a conductivity drop concomitant with the reversion back to the low-temperature ordered structure for $LiCB_9H_{10}$. The activation energies for conduction are 0.29 eV and 0.20 eV for $LiCB_9H_{10}$ and $NaCB_9H_{10}$, respectively.

We note that these activation energies may not coincide with the cation jump barriers derived from the nuclear spin-lattice relaxation measurements. This aspect was discussed in our previous work on $Na_2B_{10}H_{10}$.[4] The NMR-derived barriers reflect the average microscopic barriers for all cation jumps between the different near-neighbor sites. On the other hand, conductivity barriers reflect an overall rate-limiting step, such as a particular type of cation jump required to maintain cation percolation. Thus, some of the jumps contributing to the NMR-derived barriers may have little effect on the macroscopic conductivity barriers. For a number of the related ionic conductors studied previously, such as $Na_2B_{10}H_{10}$,[4] $LiCB_{11}H_{12}$,[10] and $NaCB_{11}H_{12}$,[10] the activation energies obtained from NMR measurements appear to be lower than those obtained from conductivity measurements.

It is clear that the thermal history of $NaCB_9H_{10}$ will affect its structure at room temperature. The superionic disordered phase is stable down to ≈285 K once it is formed above ≈310 K. This means that the electrolyte normally remains in its superionic-disordered phase at room temperature, but would need to be heated above 310 K before use, whenever it happened to drop below 285 K. As mentioned previously,[7] we have found that the superionic-disordered phases of all of the *closo*-borate compounds studied thus far can be stabilized at lower-than-normal temperatures (room temperature and below) by mechanically milling the materials. We are optimistic that the

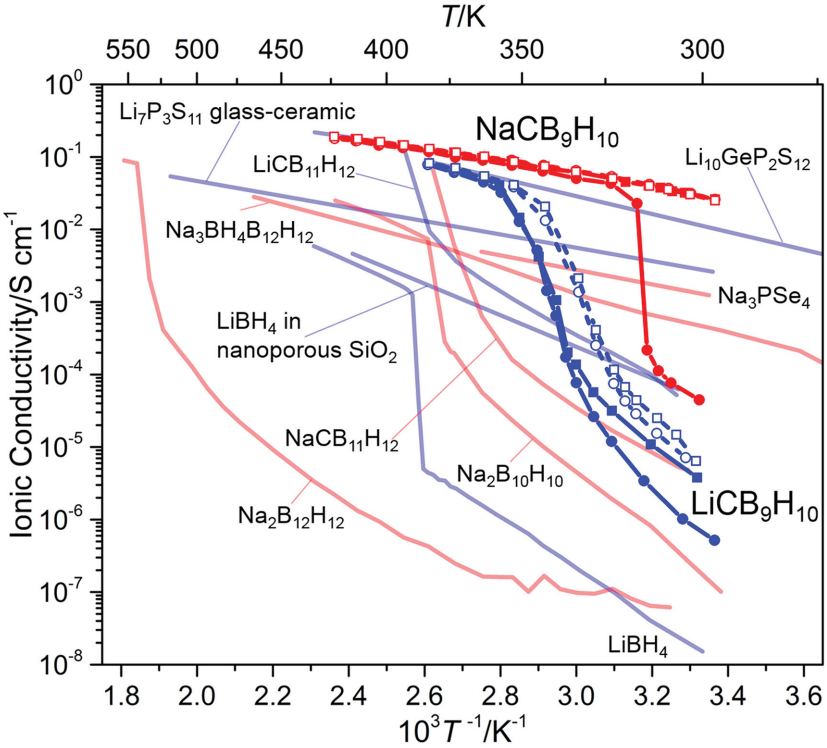

Figure 5. Ionic conductivities of $LiCB_9H_{10}$ and $NaCB_9H_{10}$ as functions of inverse temperature. Circles and squares denote the conductivities of the respective first and second temperature cycles. Closed and open symbols denote respective heating and cooling regimens. For comparison, conductivities of other select polycrystalline electrolytes are also shown: $LiCB_{11}H_{12}$,[7] $LiBH_4$,[13] $LiBH_4$ in nanoporous SiO_2,[14] $Li_{10}GeP_2S_{12}$,[15] $Li_7P_3S_{11}$ glass-ceramic,[16] $Na_2B_{12}H_{12}$,[3] $Na_2B_{10}H_{10}$,[4] $NaCB_{11}H_{12}$,[7] $Na_3BH_4B_{12}H_{12}$,[17] and Na_3PSe_4.[18]

proper morphological as well as further chemical modifications will enable us to extend the current stability ranges of the superionic phases of both $LiCB_9H_{10}$ and $NaCB_9H_{10}$ to even lower temperatures in the future.

Although similar in conductivity to their $LiCB_{11}H_{12}$ and $NaCB_{11}H_{12}$ cousins at higher temperatures, $LiCB_9H_{10}$ and $NaCB_9H_{10}$ match or surpass the best polycrystalline Li^+ and Na^+ electrolytes investigated thus far[13–18] near or at room temperature, enabled by their lower transition temperatures. Indeed, Li^+ conductivity for $LiCB_9H_{10}$ matches that of pre-sintered $Li_{10}GeP_2S_{12}$,[15] although we note that $Li_{10}GeP_2S_{12}$ that was only cold-pressed (similar to $LiCB_9H_{10}$) actually displayed a 40% reduced conductivity.[19] $NaCB_9H_{10}$ is even more impressive, displaying a room-temperature Na^+ conductivity over 20× better than for the recently reported Na_3PSe_4 chalcogenide[18] and about 60× better than for $Na_3BH_4B_{12}H_{12}$.[17]

Preliminary cyclic voltammetry measurements indicate that only cathodic and anodic currents are observed near 0 V corresponding to Li/Na deposition on the Au electrode and Li/Na stripping, respectively, without significant anodic currents, at least up to 5 V for both $LiCB_9H_{10}$ (363 K) and $NaCB_9H_{10}$ (303 K) (see Figure S7, Supporting Information). These results once again suggest favorable behaviors for these types of *closo*-borate compounds as practical solid-state ionic conductors for electrochemical applications,[7,20] although further detailed investigations are necessary to thoroughly characterize the stabilities.

The similar conductivity behaviors with temperature for $LiCB_9H_{10}$ and $NaCB_9H_{10}$ compared to those for $LiCB_{11}H_{12}$ and $NaCB_{11}H_{12}$, and their order-of-magnitude enhancements over disordered $Na_2B_{10}H_{10}$, irrespective of structural symmetries, further reinforces the notion that anion monovalency better facilitates high cation translational mobility in these large-polyhedral-anion-based systems. Indeed, the halved anion charge with respect to divalent analogs likely leads to a weaker cation–anion coulombic interaction and a low cation diffusional barrier as evidenced by NMR, where the value determined here for disordered $NaCB_9H_{10}$ (153(7) meV) is about 20% lower than that for disordered $Na_2B_{10}H_{10}$ (190(10) meV).[4] Even more noteworthy is the significantly weaker barrier determined here for $LiCB_9H_{10}$ (55(9) meV). This is also in qualitative agreement with the relative Mulliken charges on the H atoms of the isolated $CB_9H_{10}^-$ and $B_{10}H_{10}^{2-}$ anions shown in Figure 1; all the H atoms of the former have net positive charges, whereas all the H atoms of the latter have net negative charges. Thus, one might expect the surrounding cations to have overall relatively weaker interactions with the positively polarized H vertices of the $CB_9H_{10}^-$ anions than with the negatively polarized H vertices of the $B_{10}H_{10}^{2-}$ anions. Besides differences in interactions, monovalency also means that there are half as many cations required per anion for compound charge neutrality, resulting in more vacant cation sublattices and less cation-site blocking within the disordered structures. Again as the QENS results suggest, less near-neighbor cations, on average, surrounding and interacting with each monovalent anion should lead to lower anion reorientational barriers and relatively more orientationally mobile anions. As in all of these related systems, this increased anion orientational mobility may be a cooperative enabler of more facile cation transport, leading to higher ionic conductivity. Still, despite these experimental observations, a comprehensive first-principles/molecular dynamics computational study is yet required to fully understand the relative importance of anion size, valency, and reorientational mobility on the ultimate ionic conductivities attainable for this class of solid electrolyte materials.

In conclusion, this work shows that $LiCB_9H_{10}$ and $NaCB_9H_{10}$ compounds exhibit the most impressive superionic conductivities yet amongst complex-hydride-based materials,[21] including this class of large-polyhedral-anion-based salts. Moreover, the pseudoaromatic nature of the $CB_9H_{10}^-$ anions makes them relatively stable like their $B_{12}H_{12}^{2-}$, $B_{10}H_{10}^{2-}$, and $CB_{11}H_{12}^{2-}$ cousins, rendering their salts prime candidates for incorporation into next-generation, all-solid-state devices.

Experimental Section

$LiCB_9H_{10}{\cdot}xH_2O$ and $NaCB_9H_{10}$ were obtained from Katchem.[22] The main impurity in both materials was the $CB_{11}H_{12}^-$ anion, at about 6 mol% and 3 mol% in $LiCB_9H_{10}$ and $NaCB_9H_{10}$, respectively. (N.B., like other lithium and sodium *closo*-borate salt compounds containing $B_{12}H_{12}^{2-}$, $B_{10}H_{10}^{2-}$, and $CB_{11}H_{12}^-$ anions, the current compounds are air-stable, yet very hygroscopic. As their particular toxicity is not yet firmly established, it is best to practice caution when handling these materials.) Anhydrous materials were typically prepared by hours of evacuation between 433 and 473 K. Thermogravimetric analysis (TGA)/DSC measurements were made with a Netzsch (STA 449 F1 Jupiter) TGA-DSC under He using Al pans. XRPD measurements were performed using a Rigaku Ultima III X-ray diffractometer with a CuKα source. QENS measurements were performed at the NIST Center for Neutron Research on the Disc Chopper Spectrometer using thin flat-plate sample geometries in reflection, with an incident neutron wavelength of 8 Å (30 μeV fwhm resolution). ^{23}Na and ^{7}Li NMR measurements were performed on the pulse spectrometer described elsewhere[2] at resonance frequencies of $\omega/(2\pi) = 23$ MHz and 28 MHz, respectively. Nuclear spin-lattice relaxation rates were measured using the saturation-recovery method. NMR spectra were recorded by Fourier transforming the solid-echo signals. Ionic conductivities were determined in heating and cooling runs under Ar repeatedly by the AC complex impedance method using a HIOKI 3532-80 chemical impedance meter over a frequency range of 4 Hz to 1 MHz. The powder sample was pressed into a 5 mm diameter pellet of ≈1.5 mm in thickness without sintering. Besides Au foils, Li and Na foils were used as electrodes for $LiCB_9H_{10}$ and $NaCB_9H_{10}$, respectively, and mechanically fixed onto both pellet faces. Cyclic voltammetry measurements were conducted at scan rates of 0.1 mV s^{-1} and 5 mV s^{-1} using a potentiostat/galvanostat (Princeton VersaSTAT4). Mulliken atomic charges (Figure 1) for the isolated $CB_9H_{10}^-$ and $B_{10}H_{10}^{2-}$ anions were determined from first-principles calculations described in the Supporting Information. For all figures, standard uncertainties are commensurate with the observed scatter in the data, if not explicitly designated by vertical error bars.

Supporting Information

Supporting Information is available from the Wiley Online Library or from the authors.

Acknowledgements

This work was performed, in part, in collaboration between members of IEA HIA Task 32– Hydrogen-based Energy Storage. The authors gratefully acknowledge support from the Nanostructures for Electrical Energy Storage (NEES), an Energy Frontier Research Center funded by

the US Department of Energy, Office of Science, Basic Energy Sciences under Award number DESC0001160; the Collaborative Research Center on Energy Materials, Tohoku University; the Advanced Low Carbon Technology Research and Development Program (ALCA) from the Japan Science and Technology Agency (JST); JSPS KAKENHI under Grant Nos. 25220911 and 26820311; the Russian Federal Agency of Scientific Organizations under Program "Spin" No. 01201463330; and the Russian Foundation for Basic Research under Grant No. 15-03-01114. This work utilized facilities supported in part by the NSF under Agreement No. DMR-0944772. Sandia is a multi-program laboratory operated by Sandia Corporation, a Lockheed Martin Company, for the US DOE National Nuclear Security Administration under Contract DE-AC04-94AL85000.

Received: November 10, 2015
Revised: December 15, 2015
Published online:

[1] N. Verdal, J.-H. Her, V. Stavila, A. V. Soloninin, O. A. Babanova, A. V. Skripov, T. J. Udovic, J. J. Rush, *J. Solid State Chem.* **2014**, *212*, 81.
[2] A. V. Skripov, O. A. Babanova, A. V. Soloninin, V. Stavila, N. Verdal, T. J. Udovic, J. J. Rush, *J. Phys. Chem. C* **2013**, *117*, 25961.
[3] T. J. Udovic, M. Matsuo, A. Unemoto, N. Verdal, V. Stavila, A. V. Skripov, J. J. Rush, H. Takamura, S. Orimo, *Chem. Commun.* **2014**, *50*, 3750.
[4] T. J. Udovic, M. Matsuo, W. S. Tang, H. Wu, V. Stavila, A. V. Soloninin, R. V. Skoryunov, O. A. Babanova, A. V. Skripov, J. J. Rush, A. Unemoto, H. Takamura, S. Orimo, *Adv. Mater.* **2014**, *26*, 7622.
[5] M. Paskevicius, M. P. Pitt, D. H. Brown, D. A. Sheppard, S. Chumphongphan, C. E. Buckley, *Phys. Chem. Chem. Phys.* **2013**, *15*, 15825.
[6] H. Wu, W. S. Tang, V. Stavila, W. Zhou, J. J. Rush, T. J. Udovic, *J. Phys. Chem. C* **2015**, *119*, 6481.
[7] W. S. Tang, A. Unemoto, W. Zhou, V. Stavila, M. Matsuo, H. Wu, S. Orimo, T. J. Udovic, *Energy Environ. Sci.* **2015**, *8*, 3637.
[8] W. H. Knoth, *J. Am. Chem. Soc.* **1967**, *89*, 1274.
[9] H. Wu, W. S. Tang, W. Zhou, V. Stavila, J. J. Rush, T. J. Udovic, *CrystEngComm* **2015**, *17*, 3533.
[10] A. V. Skripov, R. V. Skoryunov, A. V. Soloninin, O. A. Babanova, W. S. Tang, V. Stavila, T. J. Udovic, *J. Phys. Chem. C* **2015**, *119*, 26912.
[11] R. D. Shannon, *Acta Cryst.* **1976**, *A32*, 751.
[12] N. Verdal, T. J. Udovic, V. Stavila, W. S. Tang, J. J. Rush, A. V. Skripov, *J. Phys. Chem. C* **2014**, *118*, 17483.
[13] M. Matsuo, Y. Nakamori, S. Orimo, H. Maekawa, H. Takamura, *Appl. Phys. Lett.* **2007**, *91*, 224103.
[14] D. Blanchard, A. Nale, D. Sveinbjörnsson, T. M. Eggenhuisen, M. H. W. Verkuijlen, Suwarno, T. Vegge, A. P. M. Kentgens, P. E. de Jongh, *Adv. Funct. Mater.* **2015**, *25*, 184.
[15] N. Kamaya, K. Homma, Y. Yamakawa, M. Hirayama, R. Kanno, M. Yonemura, T. Kamiyama, Y. Kato, S. Hama, K. Kawamoto, A. Mitsui*Nat. Mater.* **2011**, *10*, 682.
[16] F. Mizuno, A. Hayashi, K. Tadanaga, M. Tatsumisago, *Adv. Mater.* **2005**, *17*, 918.
[17] Y. Sadikin, M. Brighi, P. Schouwink, R. Černý, *Adv. Energy Mater.* **2015**, *5*, 1501016.
[18] L. Zhang, K. Yang, J. Mi, L. Lu, L. Zhao, L. Wang, Y. Li, H. Zeng, *Adv. Energy Mater.* **2015**, *5*, 1501294.
[19] F. Han, T. Gao, Y. Zhu, K. J. Gaskell, C. Wang, *Adv. Mater.* **2015**, *27*, 3473.
[20] A. Unemoto, T. Ikeshoji, S. Yasaku, M. Matsuo, V. Stavila, T. J. Udovic, S. Orimo, *Chem. Mater.* **2015**, *27*, 5407.
[21] a) M. Matsuo, S. Orimo, *Adv. Energy Mater.* **2011**, *1*, 161; b) A. Unemoto, M. Matsuo, S. Orimo, *Adv. Funct. Mater.* **2014**, *24*, 2267.
[22] The mention of all commercial suppliers in this paper is for clarity and does not imply the recommendation or endorsement of these suppliers by NIST.

ADVANCED ENERGY MATERIALS

Supporting Information

for *Adv. Energy Mater.*, DOI: 10.1002/aenm.201502237

Liquid-Like Ionic Conduction in Solid Lithium and Sodium Monocarba-*closo*-Decaborates Near or at Room Temperature

Wan Si Tang, Motoaki Matsuo, Hui Wu, Vitalie Stavila, Wei Zhou, Albert Alec Talin, Alexei V. Soloninin, Roman V. Skoryunov, Olga A. Babanova, Alexander V. Skripov, Atsushi Unemoto, Shin-Ichi Orimo,* and Terrence J. Udovic**

Supporting Information

Liquid-like Ionic Conduction in Solid Lithium and Sodium Monocarba-*closo*-decaborates near or at Room Temperature

Wan Si Tang, Motoaki Matsuo, Hui Wu, Vitalie Stavila, Wei Zhou, A. Alec Talin, Alexei V. Soloninin, Roman V. Skoryunov, Olga A. Babanova, Alexander V. Skripov, Atsushi Unemoto, Shin-ichi Orimo,* and Terrence J. Udovic**

X-ray Powder Diffraction Measurements

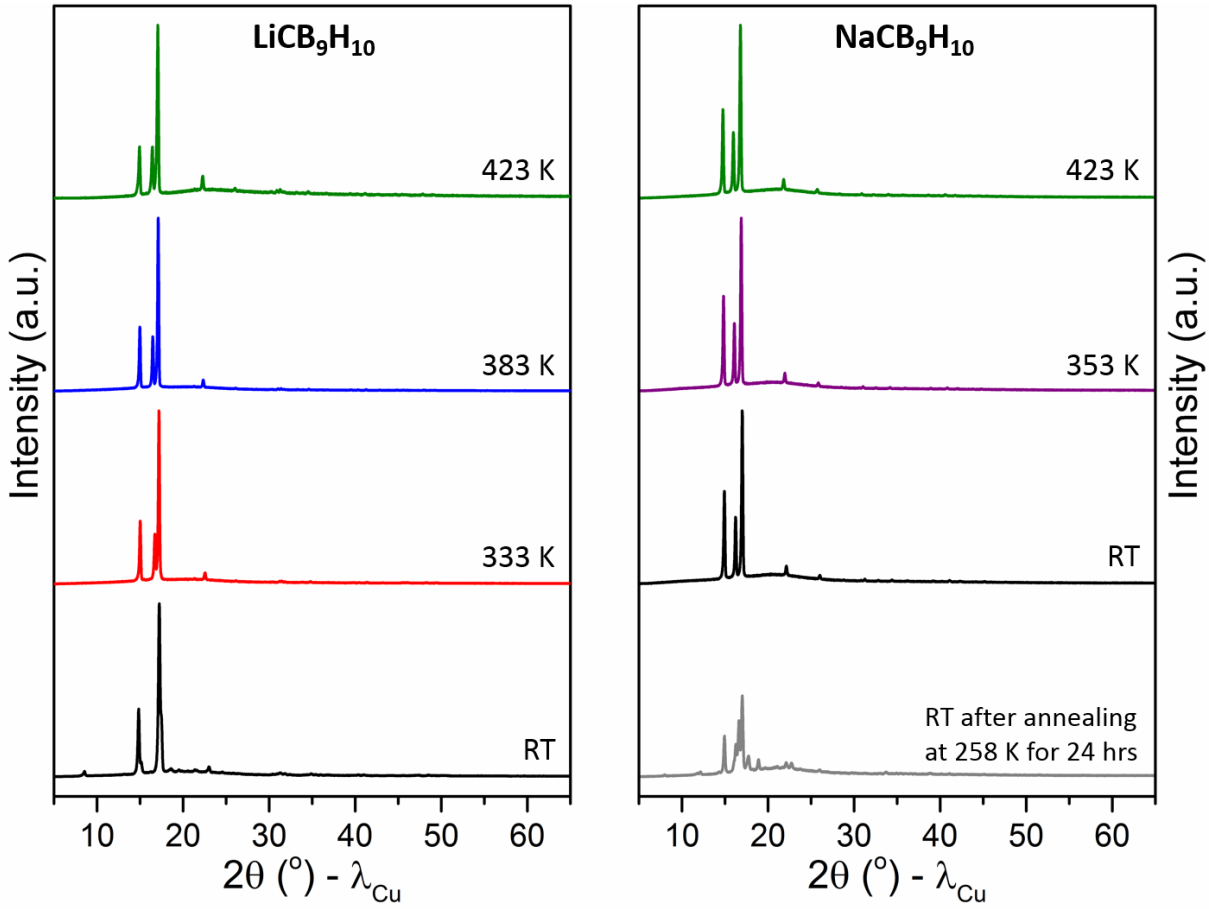

Figure S1. Experimental XRPD patterns of $LiCB_9H_{10}$ and $NaCB_9H_{10}$ vs. temperature.

Due to the laboratory XRPD limit and data quality, the cation positions and occupancies in the disordered structures cannot be rigorously determined. Therefore, complete accurate Rietveld refinement cannot be performed using the current laboratory XRPD data. Instead, comparisons of the observed XRPD patterns and the calculated patterns based on the proposed disordered models for the high-*T* phases of $LiCB_9H_{10}$ and $NaCB_9H_{10}$ are shown below.

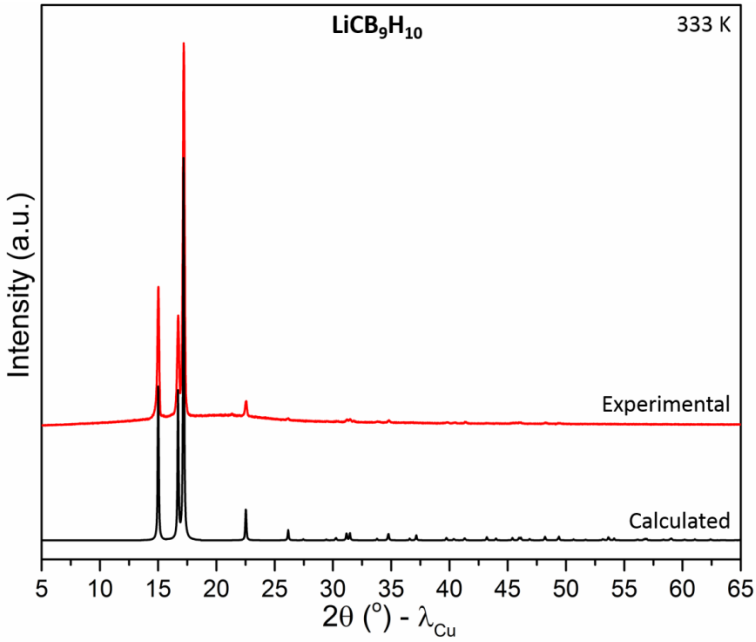

Figure S2. Experimental XRPD pattern of $LiCB_9H_{10}$ at 333 K vs. calculated pattern based on the proposed disordered orthorhombic structure model (*Cmc*2_1; *a*= 6.807 Å, *b*=11.819 Å, *c*=10.604 Å, V= 853.0 Å^3).

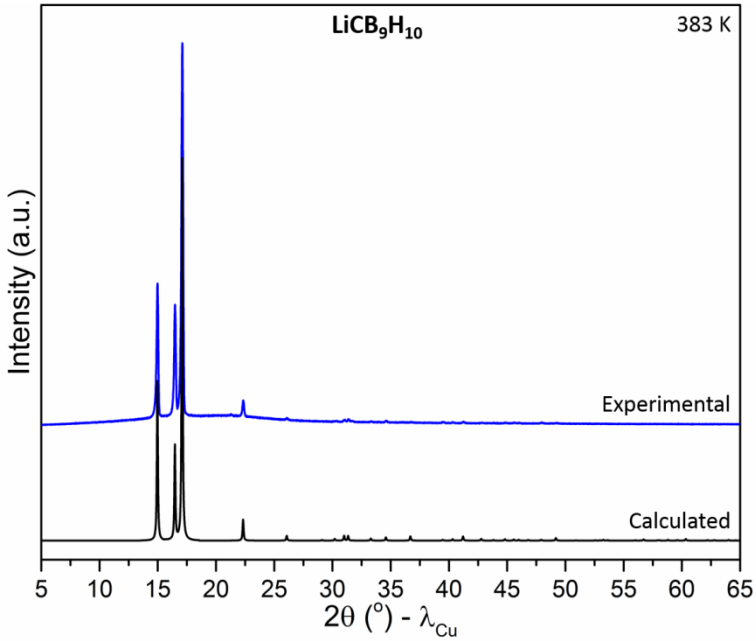

Figure S3. Experimental XRPD pattern of $LiCB_9H_{10}$ at 383 K vs. calculated pattern based on the proposed disordered hexagonal structure model (*P*3_1*c*; *a*= 6.829 Å, *c*= 10.754 Å, V= 434.3 Å^3).

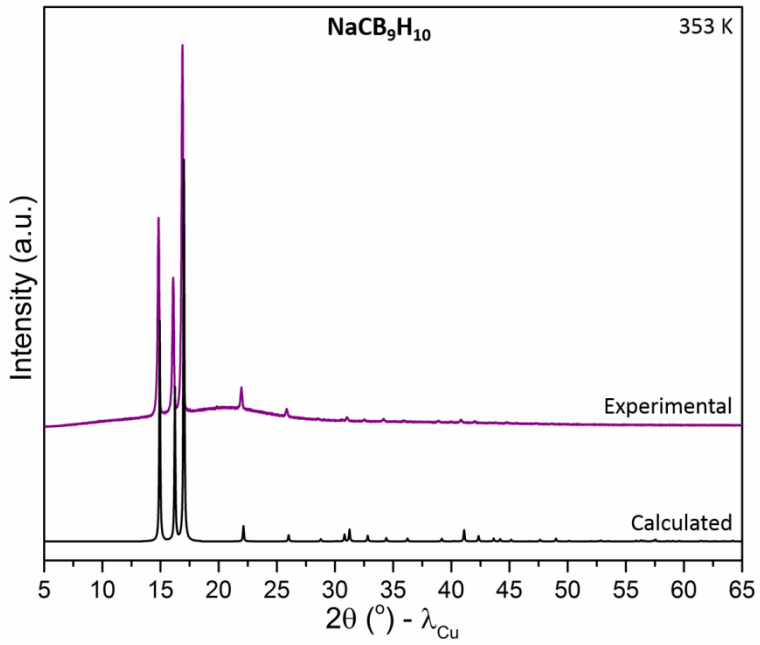

Figure S4. Experimental XRPD pattern of $NaCB_9H_{10}$ at 353 K vs. calculated pattern based on the proposed disordered hexagonal structure model. ($P3_1c$; a= 6.844 Å, c= 10.908 Å, V= 442.5 Å^3).

Quasielastic Neutron Scattering Measurements

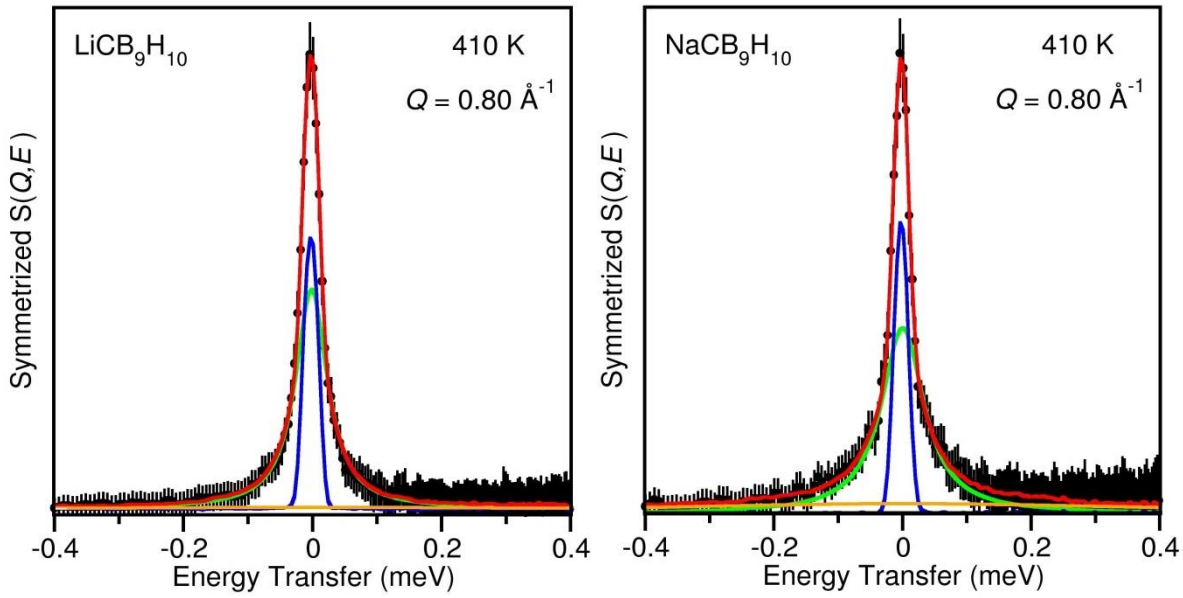

Figure S5. Representative QENS spectra for $LiCB_9H_{10}$ and $NaCB_9H_{10}$ at 410 K and Q = 0.80 Å^{-1} using 8 Å wavelength incident neutrons (30 μeV fwhm resolution). Red, blue, green, and orange curves are the overall fit to the data (black), the resolution function, the narrow Lorentzian component, and the broad Lorentzian component, respectively. The Lorentzian components are convoluted with the resolution function. The respective narrow and broad Lorentzian linewidths (fwhm) shown are 60 μeV and 0.8 meV for $LiCB_9H_{10}$ and 80 μeV and 1 meV for $NaCB_9H_{10}$.

Cole-Cole and Cyclic Voltammetry Measurements

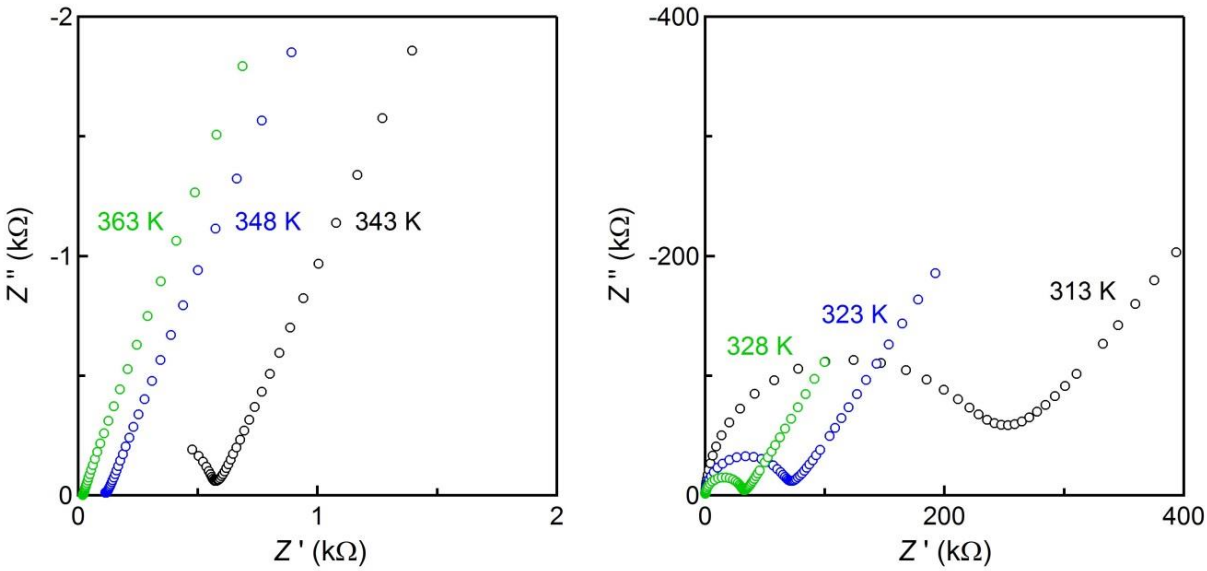

Figure S6. Complex impedance plots of the Au-symmetric cell for $LiCB_9H_{10}$ at some selected temperatures during 1st heating.

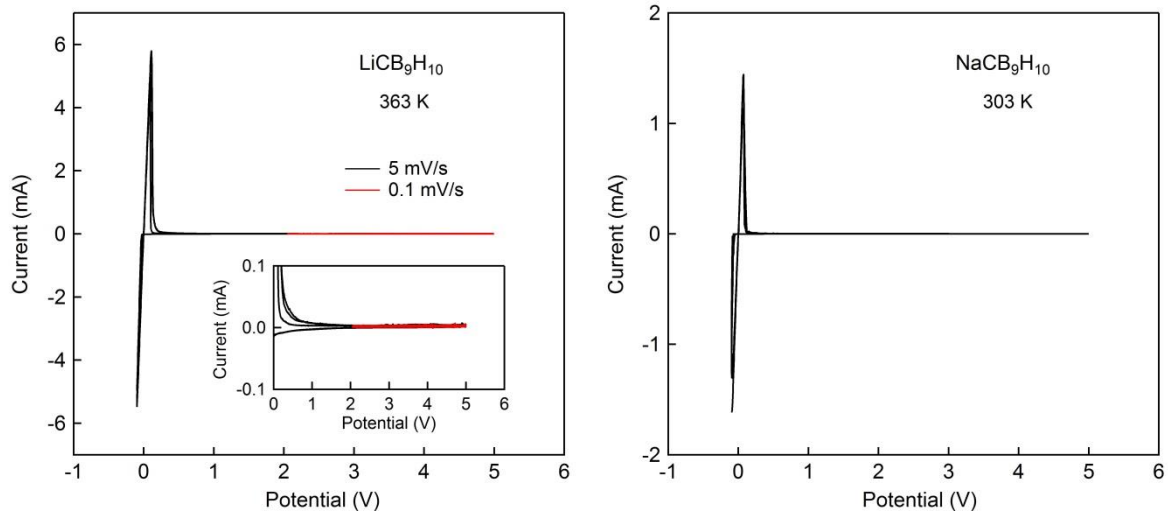

Figure S7. Cyclic voltammetry data (at 5 mV/s) for the high-*T* disordered hexagonal phases of $LiCB_9H_{10}$ and $NaCB_9H_{10}$. The measurements were repeated five times at 363 K and 303 K (after heating to 423 K) for $LiCB_9H_{10}$ and $NaCB_9H_{10}$, respectively. Data for $LiCB_9H_{10}$ is also shown at a 0.1 mV/s scan rate. The inset shows an enlarged part of the graph.

Mulliken Atomic Charge Calculations

Mulliken atomic charges (Figure 1) for the isolated $CB_9H_{10}^-$ and $B_{10}H_{10}^{2-}$ anions were determined from first-principles calculations performed within the plane-wave implementation of the generalized gradient approximation to Density Functional Theory (DFT) using a Vanderbilt-type ultrasoft potential with Perdew–Burke–Ernzerhof exchange

correlation (see P. Giannozzi, *et al. J. Phys.: Condens. Matter* **2009**, *21*, 395502). A cutoff energy of 544 eV and a 2×2×1 k-point mesh (generated using the Monkhorst-Pack scheme) were used and found to be enough for the total energy to converge within 0.01 meV $atom^{-1}$. A 30×30×30 supercell and full C_{4v} and D_{4d} molecular symmetries were used, respectively, for the $CB_9H_{10}^-$ and $B_{10}H_{10}^{2-}$ anions.